Protein Science (1993), *2*, 814-825. Cambridge University Press. Printed in the USA.

Comparison of the crystal structures of genetically engineered human manganese superoxide dismutase and manganese superoxide dismutase from *Thermus thermophilus*: Differences in dimer-dimer interaction

ULRIKE G. WAGNER,[1] KATHERINE A. PATTRIDGE,[2] MARTHA L. LUDWIG,[2] WILLIAM C. STALLINGS,[2,5] MOSHE M. WERBER,[3] CHRISTIAN OEFNER,[4,6] FELIX FROLOW,[1] AND JOEL L. SUSSMAN[1]

[1] Department of Structural Biology, The Weizmann Institute of Science, Rehovot 76100, Israel
[2] Biophysics Research Division, Institute of Science and Technology, University of Michigan, Ann Arbor, Michigan 48109-2099
[3] Bio-Technology General (Israel), Kiryat Weizmann, 76326 Rehovot 76326, Israel
[4] F. Hoffmann-LaRoche Ltd., Central Research Units, CH-4002 Basel, Switzerland

(RECEIVED November 10, 1992; REVISED MANUSCRIPT RECEIVED February 4, 1993)

Abstract

The three-dimensional X-ray structure of a recombinant human mitochondrial manganese superoxide dismutase (MnSOD) (chain length 198 residues) was determined by the method of molecular replacement using the related structure of MnSOD from *Thermus thermophilus* as a search model. This tetrameric human MnSOD crystallizes in space group $P2_12_12$ with a dimer in the asymmetric unit (Wagner, U.G., Werber, M.M., Beck, Y., Hartman, J.R., Frolow, F., & Sussman, J.L., 1989, *J. Mol. Biol. 206*, 787-788). Refinement of the protein structure (3,148 atoms with Mn and no solvents), with restraints maintaining noncrystallographic symmetry, converged at an *R*-factor of 0.207 using all data from 8.0 to 3.2 Å resolution and group thermal parameters. The monomer-monomer interactions typical of bacterial Fe- and Mn-containing SODs are retained in the human enzyme, but the dimer-dimer interactions that form the tetramer are very different from those found in the structure of MnSOD from *T. thermophilus*. In human MnSOD one of the dimers is rotated by 84° relative to its equivalent in the thermophile enzyme. As a result the monomers are arranged in an approximately tetrahedral array, the dimer-dimer packing is more intimate than observed in the bacterial MnSOD from *T. thermophilus*, and the dimers interdigitate. The metal-ligand interactions, determined by refinement and verified by computation of omit maps, are identical to those observed in *T. thermophilus* MnSOD.

Keywords: dimer-dimer interaction; human Mn superoxide dismutase; recombinant metalloenzyme; tetrameric enzyme; X-ray structure

Superoxide dismutases (SODs) are metalloenzymes that catalyze the dismutation of superoxide according to the overall equation

$$2O_2^- + 2H^+ \rightarrow O_2 + H_2O_2.$$

The reaction proceeds in two steps with cyclic reduction and reoxidation of the metal ion (Klug-Roth et al., 1973; McAdam et al., 1977; Bull & Fee, 1985; Bull et al., 1991), which is essential for activity. Superoxide dismutases are classified into two families according to the nature of the essential metals: the Mn- and Fe-containing enzymes belong to one family, with strong sequence and structural homology (Steinman, 1982; Bjerrum, 1987; Chan et al., 1990; Stallings et al., 1991), whereas the second family of Cu- and Zn-containing enzymes is distinctly different

Reprint requests to: Joel L. Sussman, Department of Structural Biology, The Weizmann Institute of Science, Rehovot 76100, Israel.
[5] Present address: Physical Sciences Center, Monsanto BB4K, 700 Chesterfield Village, St. Louis, Missouri 63198.
[6] Visiting Scientist at The Weizmann Institute of Science.

(Tainer et al., 1982) and bears no homology to the Mn-, Fe- class of dismutases.

The reported roles of superoxide radicals in ischemia–reperfusion injury, inflammatory response, chemical toxicity, and radiation damage have led to the suggestion that superoxide dismutases be employed as therapeutic agents (Bannister et al., 1987; McCord, 1988; Parizada et al., 1990; Gorecki et al., 1991), and have prompted the cloning and expression of human manganese superoxide dismutase (Beck et al., 1988). Human MnSOD is an enzyme with a subunit molecular weight of 22,200 daltons, consisting of 198 amino acids of known sequence (Barra et al., 1984; Beck et al., 1987).

Two refined X-ray structures of bacterial Mn-containing superoxide dismutases have been reported (Stallings et al., 1985, 1991; Parker & Blake, 1988; Ludwig et al., 1991). However, the amino acid sequence of the human mitochondrial enzyme, the optimal protein for clinical applications, differs from the bacterial enzymes sufficiently (less than 50% homology) to warrant an independent study of its structure. In this paper we describe the three-dimensional structure determination and refinement of recombinant human mitochondrial MnSOD at 3.2 Å resolution, and compare it to the structure of bacterial MnSOD from *Thermus thermophilus*. A parallel analysis of the structure of the recombinant enzyme has been carried out by Borgstahl et al. (1992), and the enzyme purified from human liver has been studied by Deutsch et al. (1991).

Fe- and MnSODs are composed of chains about 200 residues in length with a high proportion of residues belonging to α-helices. Current structural evidence indicates that these enzymes all form similar dimers with monomer–monomer interfaces utilizing invariant and conserved residues located near the metal ions (Stallings et al., 1985; Carlioz et al., 1988; Parker & Blake, 1988; Stoddard et al., 1990; Ludwig et al., 1991). In some species or tissues the dimers self-associate further to form tetramers: the tetrameric form is found in mitochondrial MnSODs from yeast and from higher eukaryotes, and also in a few bacterial species including the extreme thermophiles *T. thermophilus* and *Thermus aquaticus*. Recent studies have investigated the stability of either human (Matsuda et al., 1990; Werber & Greenstein, 1991) or bacterial (Sato & Nakazawa, 1978) tetrameric MnSODs as a function of pH, temperature, and denaturant concentration. The human enzyme can be dissociated into dimers and then monomers in the presence of increasing amounts of guanidinium chloride (Werber & Greenstein, 1991). Nevertheless, the relation between tetramer formation and function or stability has not been fully investigated for either human or *T. thermophilus* MnSOD.

Preliminary alignment of the sequence of human MnSOD with the three-dimensional structure of *T. thermophilus* MnSOD (Stallings et al., 1985) suggested that the packing of the chains into tetramers might be dissimilar in the human and thermophilic species. The present work demonstrates that in human MnSOD the conserved dimers pack together with a rotational orientation that differs by 84° from that in *T. thermophilus* MnSOD. This dramatic change in molecular structure is the result of deletions and residue exchanges in one segment of the polypeptide chains, which are otherwise highly homologous, having an overall identity of 47% in amino acid residues.

Table 1. *Refinement statistics*[a]

Coordinate set	*R*-factor	CC
A. Initial model		
X-PLOR, partial data[b], no NCS restraints	0.255	0.745
X-PLOR, no NCS restraints	0.194	0.878
B. Revised model		
X-PLOR, no NCS restraints	0.180	0.897
X-PLOR, with NCS restraints	0.210	0.865
X-PLOR, with NCS restraints, Mn included	0.207	0.866

[a] *R*-values and correlation coefficients for models with group temperature factors and for 6,266 reflections with $F > 0\sigma(F)$. NCS, noncrystallographic symmetry.
[b] 4,554 reflections, with $F > 3\sigma(F)$.

Results and discussion

After cycles of model building and restrained refinement using PROLSQ (Hendrickson & Konnert, 1980) and X-PLOR (Brünger, 1992a), the *R*-factor[1] is 20.7% (no solvents) and the linear correlation coefficient[2] is 0.866 for all unique data between 8.0 and 3.2 Å resolution (Table 1). The quality of the Fourier maps (Fig. 1), the geometry (root mean square [rms] deviations from ideal values of bond lengths and angles are 0.022 Å and 3.9°), and the Ramachandran plots indicate that the overall structure is correct. This paper describes the structure of human MnSOD and presents a comparison of the human and *T. thermophilus* MnSODs, with emphasis on the differences in dimer–dimer interactions (Fig. 2).

Monomer structure

The SOD monomer adopts a bilobed triangular shape of approximate dimensions 45 × 50 × 45 Å. The same fold is found in two FeSOD structures (Ringe et al., 1983; Stallings et al., 1983; Carlioz et al., 1988; Stoddard et al., 1990), in two bacterial MnSOD structures (Stallings et al., 1985; Parker & Blake, 1988; Ludwig et al., 1991), and in the human MnSOD structure reported here. The mono-

[1] $$R = \frac{\Sigma ||F_o| - |F_c||}{\Sigma |F_o|}.$$

[2] $$\mathrm{CC} = \frac{n\Sigma F_o F_c - \Sigma F_o \Sigma F_c}{(n\Sigma F^2{}_o - (F_o)^2)^{1/2}(n\Sigma F^2{}_c - (F_c)^2)^{1/2}}.$$

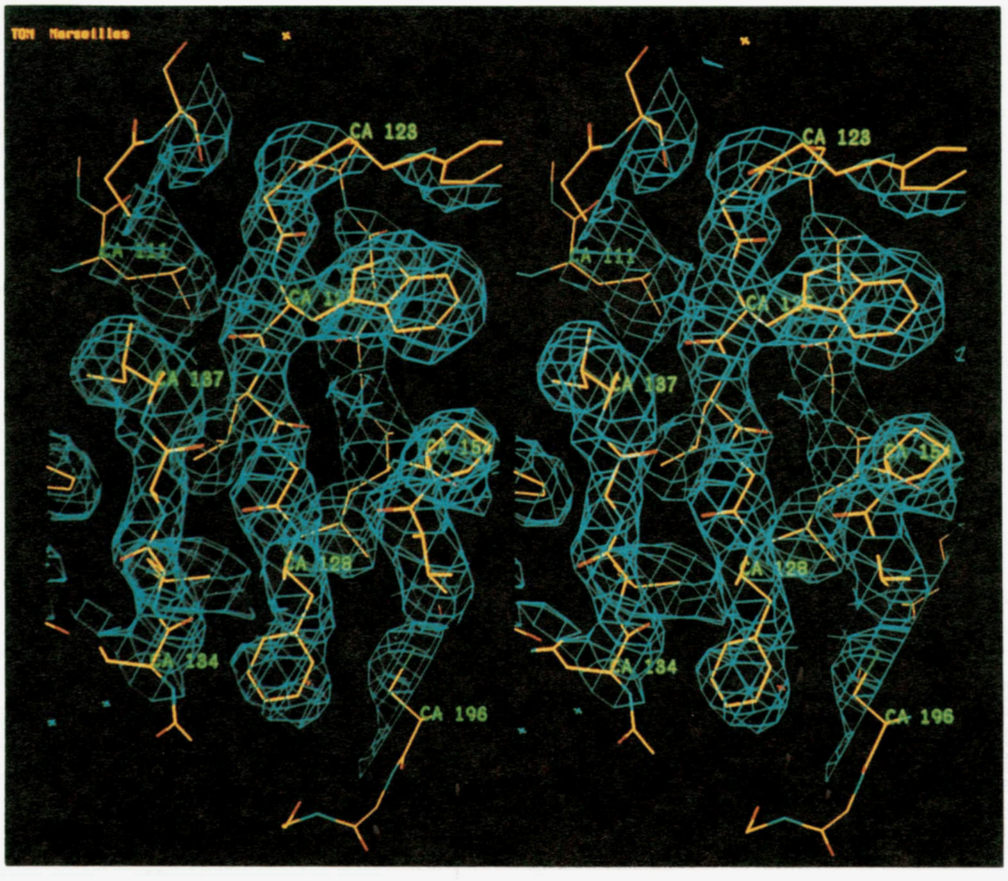

Fig. 1. Stereo view of the ($|2F_o| - |F_c|$) map of human manganese superoxide dismutase (MnSOD) in the region of the conserved β-strands, contoured at 1σ.

mer of human MnSOD comprises two distinct domains (Fig. 3). The smaller amino terminal domain includes two long antiparallel α-helices, α-1 (from residue 20 to 50) and α-3 (from residue 55 to 79), crossing each other with an angle of about 35°. The first 20 residues of this domain form an extended structure packing against the helix α-1.

As in MnSOD from *T. thermophilus*, a tight turn formed by a *cis*-Pro is found in the sequence preceding the first helix. A remarkable feature, common to all known MnSOD and FeSOD structures, is a distortion at residue His 29 in helix α-1, where an inserted residue may facilitate the juxtaposition of the invariant residues His 26, His 30, and Tyr 34 (Stallings et al., 1985). Helix α-3 in human MnSOD is kinked at Pro 62, but is not distorted at the conserved Gly-Gly-Gly sequence.

In comparison with the *T. thermophilus* dismutase, seven nonconsecutive residues are deleted from the human MnSOD sequence in the region between helices α-1 and α-3 (Fig. 2). As a result of the deletions and mismatches, the alignment of the human and bacterial enzymes is arbitrary in this region, and we expected a significant difference in the main chain fold in this part of the molecule. This portion of the structure of human MnSOD shows the largest deviation from the initial model (Figs. 3A, 4; Kinemage 1). Helices α-1 and α-3 are elongated, protruding from the surface of the monomer, and are joined by a short connector. In bacterial MnSODs, α-1 and α-3 are shorter and an additional α-helix intervenes between α-1 and α-3.

A short linker region connects the two main domains. The longer C-terminal domain includes a layer formed by three antiparallel β-strands (β-1, β-2, and β-3) flanked by four α-helices (α-4 to α-7) varying in length. The last helix, α-7, is threaded through the curved connection that links the two domains. Based on the main chain structure, β-sheets and α-helices represent 12% and 48% of the total structure, respectively.

Dimeric and tetrameric interactions

The evidence for a tetrameric structure of human MnSOD in solution comes from molecular weights determined by equilibrium sedimentation for both authentic (McCord et al., 1977) and recombinant (Beyer & Fridovich, pers. comm., 1988) human enzymes. The molecular weight for the recombinant MnSOD was found to be 81,600 ± 1,000, assuming a $\bar{v}$ value of 0.737 mL/g, which was calculated from the amino acid composition (Beyer & Fridovich,

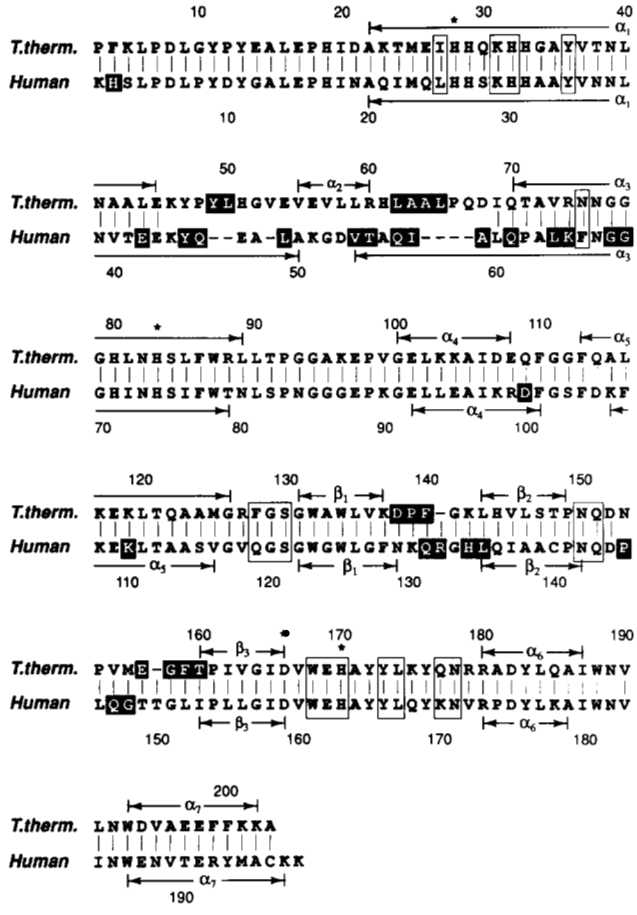

Fig. 2. Alignments of the sequences of human and *T. thermophilus* MnSODs, based on superpositions of the three-dimensional models. Structurally equivalent residues are connected by vertical lines. Secondary structural elements, as determined by the program DSSP of Kabsch and Sander (1983), are indicated. The four metal ligands are marked with asterisks. Enclosed in open boxes are the residues involved in A/B dimer contacts, which are generally conserved. Shaded boxes surround the residues involved in dimer-dimer contacts. These contacts are not conserved and occur at different positions along the chain.

pers. comm., 1988). These data were further corroborated by gel permeation chromatography experiments at various guanidinium chloride concentrations, in which it was shown that the tetramer could be dissociated into dimers at 1–2 M guanidinium chloride, whereas 4–6 M guanidinium chloride was required to obtain monomers (Werber & Greenstein, 1991).

Human MnSOD, like all the Fe- or MnSODs studied previously, crystallizes in a cell with two monomers per asymmetric unit. The chains dimerize about a noncrystallographic twofold axis, utilizing highly conserved interactions (Kinemage 2). There is no main chain penetration of one monomer into the other, but side chains extend across the boundary to form part of the packing of the opposite chain. For example, Glu 162 and Tyr 166 appear to hydrogen bond to residues in the metal-binding site of the neighboring chain, as in *T. thermophilus* (Stallings et al., 1985) and *Bacillus stearothermophilus* (Parker & Blake, 1988) MnSODs. In Figure 2 the 17 residues contributing to this dimer interface in human and in *T. thermophilus* dismutases are enclosed in boxes. Almost all of the interface residues are identical: the substitution of Phe for Gln at 119 in the human sequence is coordinated with substitution of Asn for Phe at position 66 to maintain side chain stacking of Phe with Asn or Gln in both structures. Ser 121 of the human enzyme interacts with its symmetry equivalent across the local axis, as does the corresponding Ser 130 in *T. thermophilus* MnSOD. The local packing at this interface brings the active sites close to each other; the Mn–Mn distance is 18.4 Å in *T. thermophilus* SOD and 18.1 Å in the human protein. The conserved dimers of the human and bacterial structures can be superimposed with an rms deviation of 0.84 Å for the 174 structurally conserved residues (see Figs. 2, 4).

Although the active site and the region surrounding it, as well as the monomer–monomer interface, are essentially indistinguishable in the human and bacterial enzymes, the dimer–dimer interface is completely different. Indeed, the tetrameric contacts of human MnSOD have not been previously observed for other Fe- or MnSODs, and thus constitute interesting additions to the library of dimer–dimer interfaces in tetrameric proteins (Miller, 1989). The *T. thermophilus* tetramer is relatively open, showing *mm* symmetry (Fig. 5A). In contrast, the human tetramer is more compact, showing approximate tetrahedral symmetry. The difference is due to a rotation of 84° of one dimer relative to the *T. thermophilus* structure (Fig. 5A,B; Kinemage 3). In the human MnSOD structure the interface between the two dimers is formed mainly by protruding helices, which aggregate like a four-helix antiparallel bundle (Fig. 5C; Kinemage 4). The up-down:up-down packing of residues 42–65 against the symmetry-related residues 42#–65# is generated by the symmetry operation: $-x, 1-y, z$. A second set of tetramer contacts is made by the turn between sheet strands β-2 and β-3, which fits nicely against α-3 of the symmetry-related chain and adjoins the α–α contact. The substructures of the tetramer interface are very different in *T. thermophilus* MnSOD, where a ring of short helical segments acts as a pocket to accommodate the turn at residue 140 (Ludwig et al., 1991). The packing of the dimers in the tetramer of human MnSOD is tighter than in *T. thermophilus* MnSOD, rendering the molecule more compact along the direction of the conserved local dyad, as can be seen in the schematic drawing of Figure 5A. Distances of corresponding atoms from the plane that bisects the tetramer are less by about 2.7 Å in the structure of human MnSOD.

The overall structure that we determined at 3.2 Å resolution is very similar to what was seen at 2.2 Å resolution (Borgstahl et al., 1992). The rms deviation of the 396 equivalent Cα atoms between the dimers of the two struc-

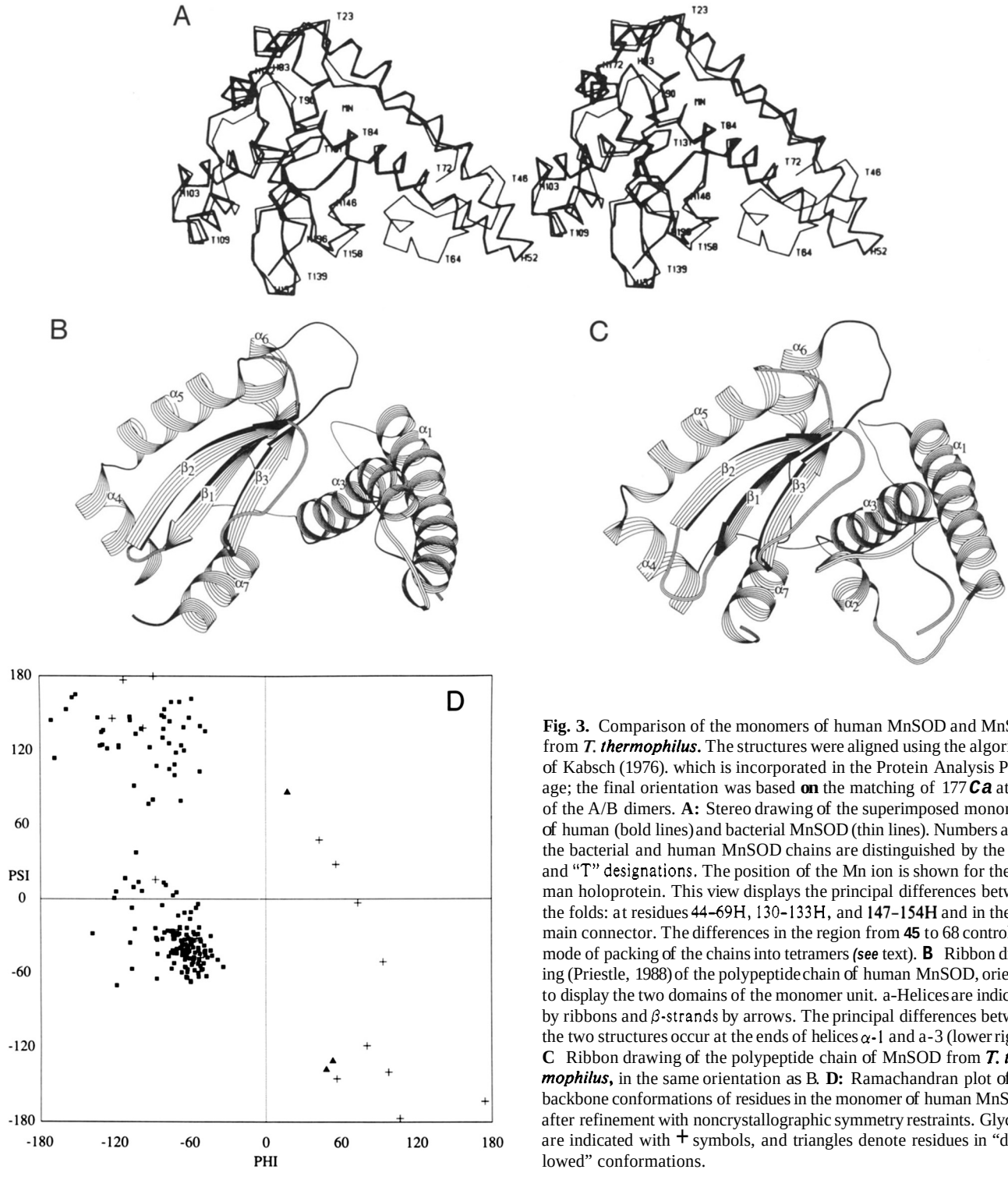

Fig. 3. Comparison of the monomers of human MnSOD and MnSOD from *T. thermophilus*. The structures were aligned using the algorithm of Kabsch (1976). which is incorporated in the Protein Analysis Package; the final orientation was based **on** the matching of 177 *Ca* atoms of the A/B dimers. **A:** Stereo drawing of the superimposed monomers of human (bold lines) and bacterial MnSOD (thin lines). Numbers along the bacterial and human MnSOD chains are distinguished by the "H" and "T" designations. The position of the Mn ion is shown for the human holoprotein. This view displays the principal differences between the folds: at residues 44–69H, 130–133H, and 147–154H and in the domain connector. The differences in the region from **45** to 68 control the mode of packing of the chains into tetramers *(see* text). **B** Ribbon drawing (Priestle, 1988) of the polypeptide chain of human MnSOD, oriented to display the two domains of the monomer unit. a-Helices are indicated by ribbons and β-strands by arrows. The principal differences between the two structures occur at the ends of helices α-1 and a-3 (lower right). **C** Ribbon drawing of the polypeptide chain of MnSOD from *T. thermophilus*, in the same orientation as B. **D:** Ramachandran plot of the backbone conformations of residues in the monomer of human MnSOD, after refinement with noncrystallographic symmetry restraints. Glycines are indicated with + symbols, and triangles denote residues in "disallowed" conformations.

ture determinations is 0.72 Å (0.49 Å for the 394 equivalent Cα, excluding the two C-termini residues). The largest difference in the structures (excluding the N- and C-termini) lies in the connection between the two domains, i.e., between a-3 and a–4, in the vicinity of residues 83–86, where equivalent C a atoms differ by up to **1.5** Å. This may be due in part to the difference in noncrystallographic restraints, in that the rms deviation in equivalent C a atoms of this determination is 0.03 Å, whereas for that of Borgstahl et al. (1992) it is **0.25** Å.

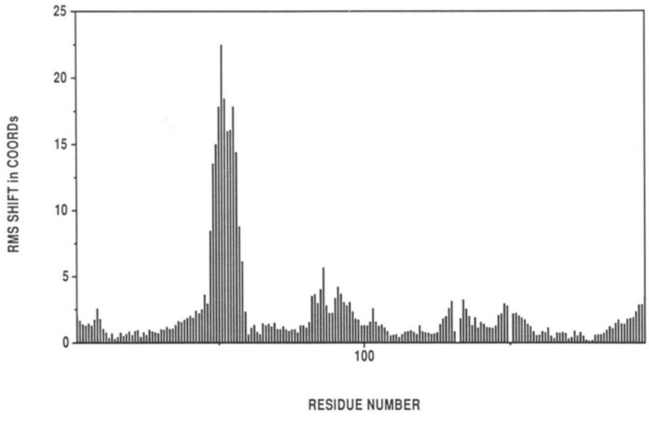

Fig. 4. Distances between Cα positions of the human and bacterial MnSODs after spatial alignment of their **A/B** dimers as described in the text. Numbering corresponds to the human sequence (see Fig. 2).

The active site

In all known bacterial Mn- and FeSOD structures, the metal is bound by four invariant protein ligands (Fig. 2; Kinemage 1): one aspartate and three histidines (Ringe et al., 1983; Stallings et al., 1983, 1985; Parker & Blake, 1988). The positions of the ligand atoms in the refined structures of ***7: thermophilus*** and ***B. stearothermophilus*** dismutases correspond approximately to the vertices of a trigonal bipyramid (Fig. 6). One of the axial positions in the Mn enzyme from ***7: thermophilus*** ($R = 0.176$ at 1.8 A resolution) is occupied by a solvent molecule (Stallings et al., 1985, 1991; Ludwig et al., 1991), whereas in the structure of ***B. stearothermophilus*** MnSOD ($R = 0.26$ at 2.4 Å resolution) this axial site appears open. The coordination geometry at Mn in human MnSOD is indistinguishable from that found in the higher resolution structure of MnSOD from ***7: thermophilus*** (Ludwig et al., 1991). The locations of the hydrophobic side chains that surround the metal–ligand cluster are all maintained: the aromatic residues, His 27, His 30, His 31, Tyr 34, Phe 77, Trp 78, Trp 125, Tyr 166, and Tyr 176 occupy essentially the same positions as their counterparts in ***7: thermophilus*** MnSOD (Stallings et al., 1985; Ludwig et al., 1991).

Crystals of human MnSOD were grown in 2-methyl-2,4-pentanediol (MPD) from preparations in which the metal content before crystallization was typically 0.65–0.85 Mn atoms per subunit (M.M. Werber, unpubl.). However, the crystals of human MnSOD appeared almost colorless, in contrast with the purple color observed for bacterial Mn(III) crystals of SODs that were grown from ammonium sulfate[3] or polyethylene glycol (Beem et al., 1976; Bridgen et al., 1976; Stallings et al., 1984; Parker & Blake, 1988). Nevertheless, Fourier and difference Fourier maps computed with and without Mn in the atomic model clearly demonstrate substantial occupancy of the metal sites (see Materials and methods). Partial reduction to Mn(II) may be responsible for the loss of the visible absorbance.

[3] Refinement of the parameters for the metal sites in MnSOD from *T. thermophilus* shows that the metal sites in this crystalline MnSOD are fully occupied (Ludwig et al., **1991).**

Materials and methods

Data collection

Recombinant human methionyl-MnSOD, expressed in ***Escherichia coli,*** was purified (Beck et al., 1988)and crystallized as previously reported (Wagner et al., 1989). The crystals diffracted to ~2.8 Å resolution, but because they were radiation sensitive, X-ray diffraction data were measured at 100 K following the cooling technique described by Hope (1988), using a Rigaku AFC5-R 4 circle rotating anode diffractometer. The cell parameters at 100 K (see below) are $a = 77.80$, $b = 74.10$, $c = 68.42$ Å, $V = 394{,}440$ Å^3, which represents a shrinkage of 3% in unit cell volume upon flash cooling from room temperature, according to data reported previously (Wagner et al., 1989). Two space groups were possible: $P2_12_12_1$ and $P2_12_12$ with a pseudo-twofold screw axis along z. The enzyme is a tetramer in solution (Beyer & Fridovich, pers. comm., 1988; Werber & Greenstein, 1991), and from density measurement, unit cell volume, and molecular weight we deduced that the asymmetric unit contains a dimer. Of the two possible space groups, only $P2_12_12$ allows the dimers to associate across a crystallographic dyad. Intensities were measured from one crystal in a series of resolution shells, using omega/two theta scans. Radiation damage was monitored by a set of reference reflections, which indicated no decay during the experiment, but data collection was terminated by loss of coolant when the data set was 98% complete to 3.2 Å.

Noncrystallographic symmetry

Using the program PROTEIN (Steigemann, 1985), with data for which $F > 3\sigma$ and a resolution of 8.0–3.5 Å, a self-rotation search (Rossmann & Blow, 1962) gave an indication for a noncrystallographic twofold axis about 11° from the y-axis. The results, however, were not conclusive (the peak height was about 53% of the origin peak; the next highest peak was 23%) and were shown to be correct only after solving the structure.

Molecular replacement

The structure was solved by the method of molecular replacement using the well-refined structure of MnSOD from ***7: thermophilus*** (Ludwig et al., 1991) as a search model. Because of the close similarity of the sequences, the entire bacterial dimeric molecule containing 3,284 atoms, with all side chains, was used for calculating model

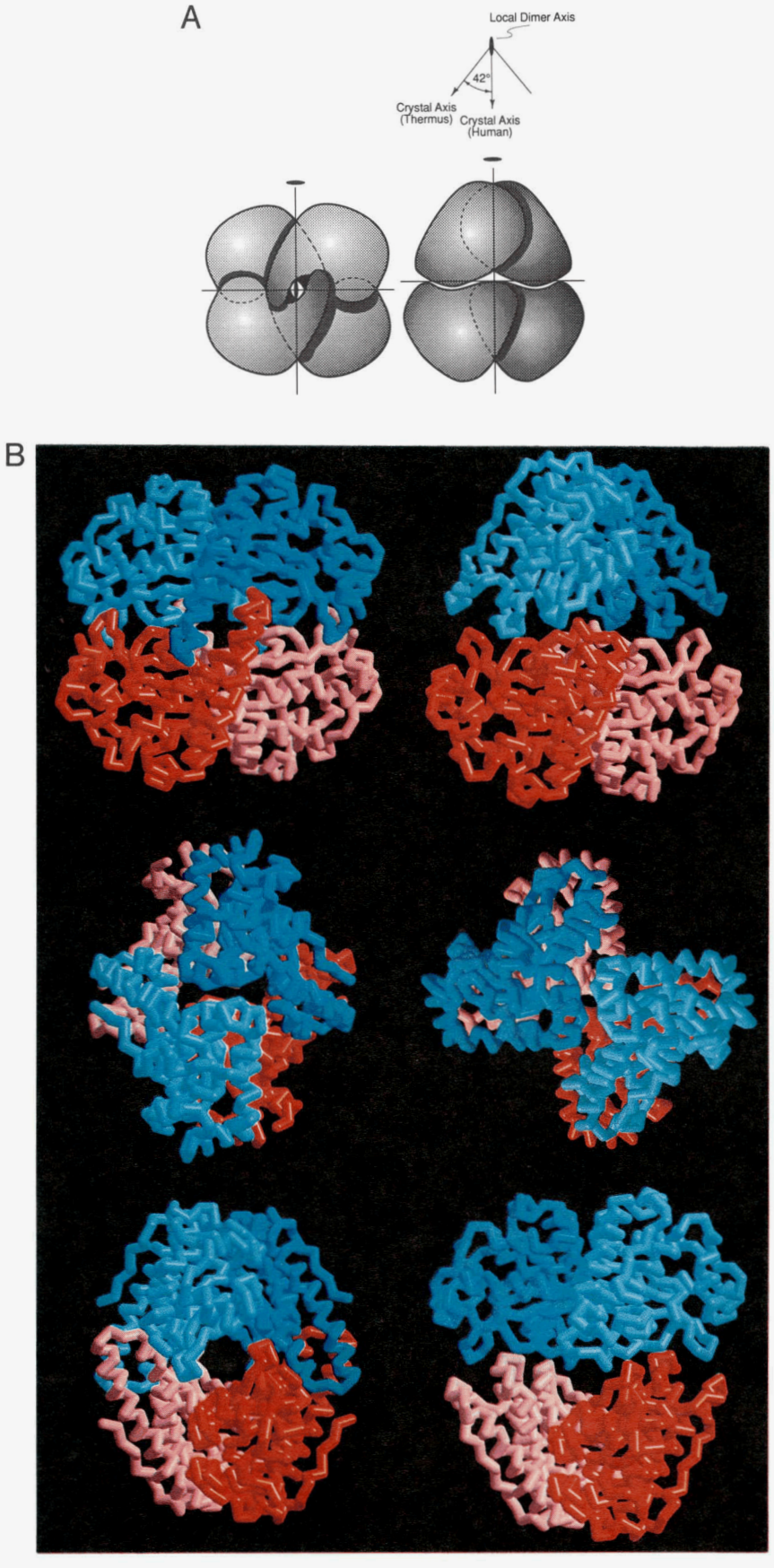

Fig. 5. *See next page for caption and balance of figure.*

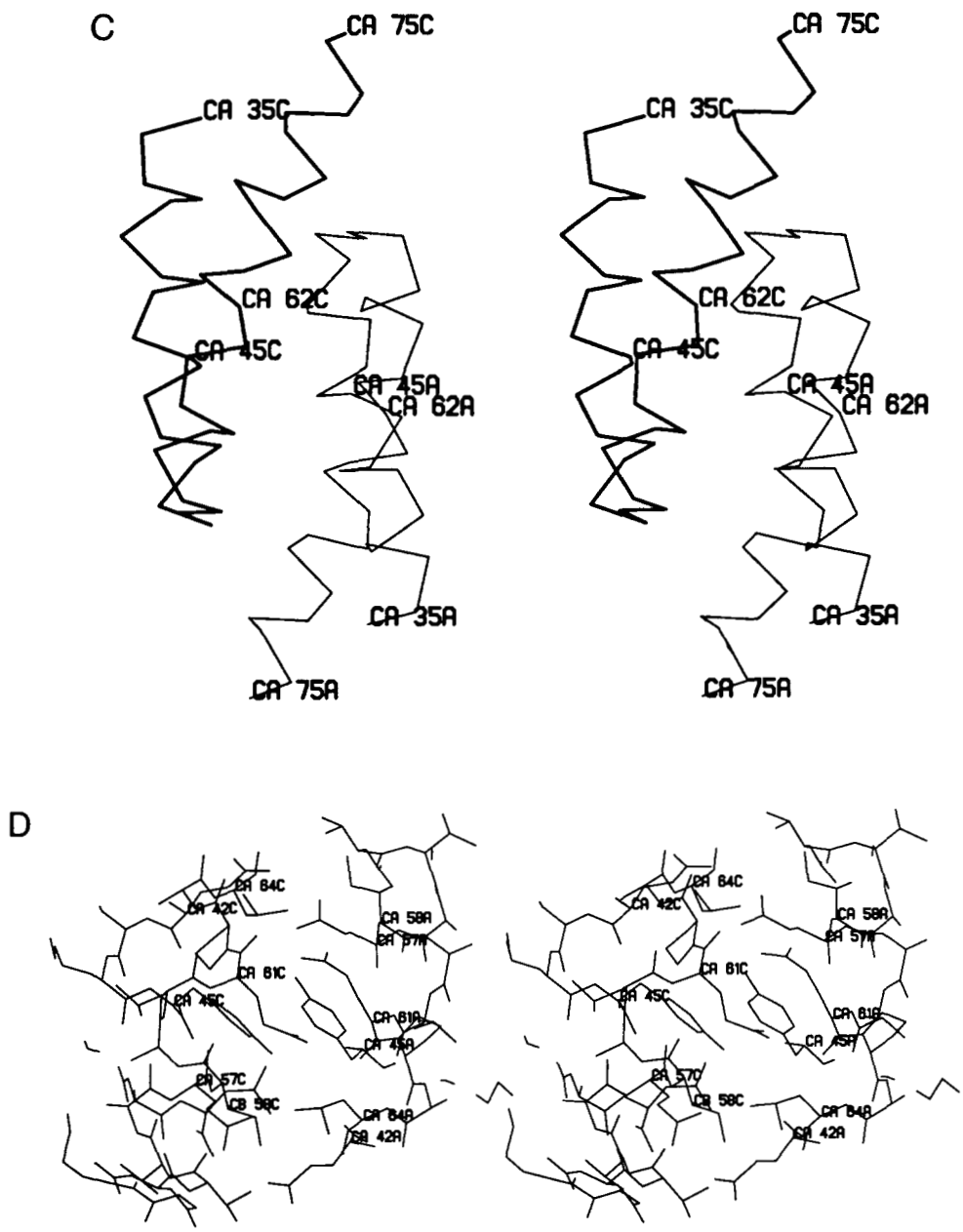

Fig. 5. Comparisons of tetramer packing in human and *T. thermophilus* MnSODs. **A** (*facing page*): Schematic drawings showing the relative orientation of the symmetry elements and the subunits in each structure. The conserved local dyads are vertical in each structure and the A/B pairs of chains (bottom) are aligned. Human MnSOD is represented on the left and *T. thermophilus* MnSOD on the right. In human MnSOD the crystallographic dyad is perpendicular to the page, but in *T. thermophilus* MnSOD it is rotated as shown in the inset, which is a perpendicular view down the local dyad. The closer packing of the dimers in human MnSOD is illustrated in this schematic comparison: the center of the human tetramer is displaced 2.73 Å from the center of the bacterial tetramer. This panel also serves as a guide to the photographs displayed in panel B. **B** (*facing page*): Cα representations of the tetramers of human MnSOD and *T. thermophilus* MnSOD, viewed down the dyad axes of human MnSOD. The structure of the human enzyme is at the left of each panel; to the right is a corresponding view of the thermophile MnSOD with the red A/B chains aligned with the red (lower) A/B chains of the human enzyme. *Top:* View down the crystallographic axis of human MnSOD. *Middle:* View down the conserved local dyad that relates two neighboring metal binding sites. Both molecules show dyad symmetry in this view, and the relative rotation of the upper (blue) pairs of chains is clearly displayed. *Bottom:* View along the third dyad of human MnSOD. **C:** Stereo drawing of the contacts responsible for tetramer formation in human MnSOD. Four helical regions from chains related by crystallographic symmetry interact in a fashion resembling four-helix bundle topologies. The crystallographic dyad is approximately perpendicular to the plane of the drawing. The tetramer contact also includes interactions between the beginning of helix α-3 and a turn (147C–150C) from the symmetry-related subunit (not shown). **D:** Details of a section through the helix interface shown in C, in the same orientation as that drawing. Symmetry-related tyrosines 45A and 45C are close to the dyad axis at the center of the drawing. The interactions of these and other side chains can be compared with Figure 6 of Borgstahl et al. (1992).

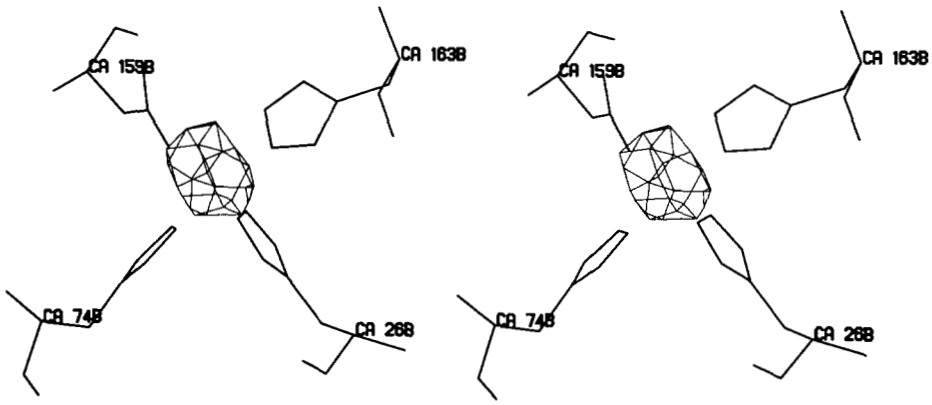

Fig. 6. Electron density in the vicinity of the Mn binding site of the B chain: difference ($|F_o| - |F_c|$) map after X-PLOR refinement of a model from which the metal ions were omitted (line 4 of Table 1). The positive contours are at 4σ; the peak density at the metal site is about 6σ.

structure factors (excluding only the Mn and solvent atoms). Computation was done with the molecular replacement program package MERLOT (Fitzgerald, 1988) running on a CONVEX C220 computer. An artificial P1 unit cell was chosen about two and a half times as large as the longest intramolecular distance in the bacterial dimer, i.e., 130 × 130 × 130 Å. An initial cross rotation search was carried out over the unique Euler rotational space using the fast rotation function CROSUM (Crowther, 1972) with a step size of 5° in β, including all data in the resolution range between 8 and 4 Å. This solution was then refined with the Lattman cross rotation program LATSUM (Lattman & Love, 1972), with all data between 8.5 and 5.3 Å, using 1.0°, 0.5°, and 0.5° steps in α, β, and γ, respectively. The rotation search was limited to an Euler space of α, 0–180°; β, 0–90°; γ, 0–180°. The translation search was performed using both a Patterson search in the Harker sections of space group $P2_12_12$ (Crowther & Blow, 1967) and an independent R-factor search (Ward et al., 1975) with data between 10 and 5.3 Å. The rotation and translation parameters were jointly refined using the R-factor minimization procedure RMINIM (Ward et al., 1975). At the end of these steps the R-factor was 0.49. Results of the searches are shown in Table 2.

Further refinement of the molecular replacement solution was carried out with the program CORELS (Sussman et al., 1977), starting from an atomic model that was modified to accord with differences in the sequences of human and thermophile SODs. As there are seven additional amino acids between the α helices 1 and 3 in the *T. thermophilus* relative to the human MnSOD sequence, we took the backbone of this part of the model from the known structure of *E. coli* FeSOD, which also has fewer residues in this region (Stallings et al., 1983). For the rest of the model the backbone from *T. thermophilus* was retained, but the side chains were replaced by Ala except for identities in the conserved helical and β-sheet regions, and where Gly is present in the human sequence. Each monomer was treated as a rigid group and allowed to rotate and translate in the asymmetric unit. The refinement converged at an R-factor of 0.42 (10–4.0 Å) after 5 cycles and 0.44 (10–3.2 Å) after 15 cycles including all data in these resolution ranges.

Refinement and model building

PROLSQ refinement

The complete structural model for human MnSOD was developed in several stages. The first stage employed restrained refinement with the program PROLSQ (Hen-

Table 2. *Results of molecular replacement*

	α (°)	β (°)	γ (°)	Peak height (rms)[a]
LATSUM	30.5	50.0	123.0	2.0
	x	y	z	Peak height (rms)[a]
TRNSUM				
$u, v, 0$	0.03	0.31	–	2.85
$0.5, v, w$	–	0.30	0.25	3.72
$u, 0.5, w$	0.04	–	0.25	4.15
	x	y	z	Peak height (rms)[a]/R[b]
RVAMAP	0.05	0.30	0.25	4.74/0.52
	α/x	β/y	γ/z	R[b]
RMINIM	29.5/0.04	50.2/0.30	122.0/0.25	0.49

[a] Peak height in units of root mean square (rms) deviation above the average value of the rotation search.

[b] $R = \dfrac{\Sigma\,||F_o| - |F_c||}{\Sigma\,|F_o|}$.

drickson & Konnert, 1980; Finzel, 1987; Sheriff, 1987) and alternating rounds of interactive model building. Electron density maps with amplitudes $(2|F_o| - |F_c|)$ and calculated phases were used to rebuild portions of the molecule where we could see density for side chains that had been modeled as Ala. Interactive fitting was performed using the computer graphics program FRODO (Jones, 1978; Pflugrath et al., 1984) on an Evans and Sutherland PS390 graphics system. All of the atoms in the protein except Mn were included in the last of these cycles.

X-PLOR refinement: Homology modeling of the conformation at the tetramer interface

Inspection of the partly refined model in the region between residues 45 and 62 revealed some very short interatomic contacts and unfavorable nonbonded interactions. This region, where the sequences of the human and thermophile MnSODs are very different, is part of the tetramer interface. The unsatisfactory stereochemistry and the rather high R and low correlation coefficient led us to continue refinement and to attempt remodeling of the interface regions. We employed a combination of simulated annealing in X-PLOR (Brünger, 1992a), omit maps, and weighted $(2|F_o| - |F_c|)$ and $(|F_o| - |F_c|)$ maps (Read, 1990) in order to improve and verify the atomic model.

The model from the initial PROLSQ and X-PLOR refinements terminated helix α-1 at Glu 47 and began helix α-3 at Gln 61, so that Pro 62 was part of the N-terminal cap of α-3. The residues intervening between helices were in several tight turns. Using $(3|F_o| - 2|F_c|)$ maps and omit maps calculated with phases from the remaining atoms (coefficients $|F_o| \exp i\alpha c$) we compared this interpretation with structures selected from the database by the routine DGLP in TOM (Cambillau & Horjales, 1987). A related region from uteroglobulin suggested an alternative model that extended helices α-1 and α-3, allowing Pro 62 to introduce a distinct kink in helix α-3 (as shown in Fig. 5C). To maintain reasonable nonbonded contact distances, we also rebuilt the adjoining turn at 148–151. Refinement of this modified model in X-PLOR, using simulated annealing with B fixed at 15.0 for all atoms, reduced R from 0.302 to 0.196 (for all $|F_o| > 0\sigma$). The stereochemistry was much more acceptable, with absence of short contacts, and the interactions at the tetramer interface were chemically reasonable.

Refinements of the alternative models are summarized in Table 1. From the results with the initial model the importance of refining against all the data is evident. The R for the partial data set was 0.190, but the model agreed poorly with the full set of data ($R = 0.255$). Although the revised model with longer helices was judged to be correct by all criteria, the substantial changes in the chain fold at residues 46–60 did not result in dramatic differences in R at the 3.2-Å limit of our resolution. We presume this is because the atoms in both models occupy similar regions in the crystal.

As a further test of the validity of the model shown in Figure 5C and D, we omitted segments of the 45–60 sequence and its local symmetry equivalents from each of the phasing models, repeated simulated annealing as described by Brünger (1992a), and examined weighted $(2|F_o| - |F_c|)$ and $(|F_o| - |F_c|)$ omit maps. Images corresponding to the modified model, with extended helices, were observed in maps where the starting phases were derived from the original model, but the "incorrect" images, with shorter helices, were not observed in maps after omit refinement starting from the "correct" model phases. In attempts to discern differences in the models by calculations of free R (Brünger, 1992b), we found that the behavior of free R (for 10% of the scattering) was almost the same for both starting models. The free R values plateaued at 0.431 and 0.417, whereas the R for reflections included in refinement decreased to 0.199 and 0.185 for the original model and for the preferred alternative model with extended helices, respectively.

To check other regions of the molecular model, where the structure appeared to be identical with MnSOD from *T. thermophilus*, we carried out positional refinements (Brünger, 1992a), omitting 10-residue segments all along the chain, and inspected the resulting omit maps. Regions that are ill-defined or may differ in the A and B chains were noted in this process: the N-terminus, the domain connector, the turn near 130, and the C-terminus. All these regions had larger than average thermal parameters. Refinement of isotropic temperature factors in X-PLOR reduced the average B from 15.0 to 11.1 Å^2. The small temperature factors seem to be a consequence of the limited resolution, rather than indicators of reduced motion at the temperature of data collection (100 K), since trimming the data from *T. thermophilus* MnSOD to 3.2 Å in control calculations yielded similarly small values for individual atom thermal factors.

The refinements with PROLSQ and X-PLOR, described above, were conducted without imposing restraints on the agreement of parameters of atoms related by noncrystallographic symmetry (NCS). Some rather large variations were observed in comparisons of the two chains composing the asymmetric unit, with the rms variation of Cα atoms being about 0.7 Å after simulated annealing and positional refinement in the absence of NCS restraints. Invoking NCS restraints resulted in an R value of 0.207 (with group B values and Mn) and rms differences in Cα coordinates of 0.025 Å, when we started from the model whose R-factor and correlation coefficients were 0.180 and 0.897, respectively, without NCS restraints (Table 1). It is the NCS restrained model that we describe in this paper.

The Mn binding site

Because the color of the crystals initially suggested loss of Mn, the PROLSQ and initial X-PLOR refinements did not include the metal ions. In the absence of the metal

the protein ligands move during refinement and the side chains rotate relative to their positions in the presence of Mn. In difference maps based on phases from the PROLSQ model (Table 2), peaks appeared at the metal sites with heights of approximately 2σ. After refinement of the revised model in the absence of NCS restraints, the peak heights reached 4σ. ($|F_o| - |F_c|$) difference maps calculated after X-PLOR refinement of the apoprotein to $R = 0.210$ with NCS restraints (see above) displayed positive peaks at the metal positions with heights of approximately 6σ (Fig. 6).

Refinement by simulated annealing (Brünger, 1992a) of a model including Mn was conducted with restraints on the metal–ligand bond lengths but with very small force constants (5.0) restraining the bond angles at the metal. Refinement of the metal occupancy was not attempted, but the B values of the metals were significantly higher than those of the ligand atoms, suggesting less than full occupancy of the metal-binding sites. The limited resolution also complicates identification of the solvent ligand that has been observed in analyses of Mn- and FeSODs (Ludwig et al., 1991).

Acknowledgments

We thank Drs. W.F. Beyer, Jr. and I. Fridovich for the information (prior to publication) on the molecular weight of the recombinant MnSOD used in this work. We gratefully acknowledge the expertise of Luisa Pugliese in growing MnSOD crystals and Orly Dym for valuable discussions. This work was supported by grants (to J.L.S.) from the United States–Israel Binational Science Foundation (BSF), Jerusalem, Israel, and the Kimmelman Center for Biomolecular Structure and Assembly, Rehovot, Israel; by fellowships (for U.G.W.) from the Feinberg Graduate School of The Weizmann Institute of Science and the Bundesministerium für Wissenschaft und Kunst, Wien, Austria; and by grant GM 6M16429 (to M.L.L.) from the National Institutes of Health.

References

Bannister, J.V., Bannister, W.H., & Rotilio, G. (1987). Aspects of the structure, function, and applications of superoxide dismutase. *Crit. Rev. Biochem. 22*(2), 111–180.

Barra, D., Schinia, M.E., Simmaco, M., Bannister, J.V., Bannister, W.H., Rotilio, G., & Bossa, F. (1984). The primary structure of human liver manganese superoxide dismutase. *J. Biol. Chem. 259*, 12595–12601.

Beck, Y., Bartfeld, D., Yavin, Z., Levanon, A., Gorecki, M., & Hartman, J.R. (1988). Efficient production of active human manganese superoxide dismutase in *Escherichia coli*. *Biotechnology 6*, 930–935.

Beck, Y., Oren, R., Amit, B., Levanon, A., Gorecki, M., & Hartman, J.R. (1987). Human Mn superoxide dismutase cDNA sequence. *Nucleic Acids Res. 15*, 9076.

Beem, K.M., Richardson, J.S., & Richardson, D.C. (1976). Manganese superoxide dismutase from *Escherichia coli* and from yeast mitochondria: Preliminary X-ray crystallographic studies. *J. Mol. Biol. 105*, 327–332.

Bjerrum, M.J. (1987). Structural and spectroscopic comparisons of manganese-containing superoxide dismutases. *Biochim. Biophys. Acta 915*, 225–237.

Borgstahl, G.E.O., Parge, H.E., Hickey, M.J., Beyer, W.F., Jr., Hallewell, R.A., & Tainer, J.A. (1992). The structure of human mitochondrial manganese superoxide dismutase reveals a novel tetrameric interface of two 4-helix bundles. *Cell 71*, 107–118.

Bridgen, J., Harris, J.L., & Kolb, E. (1976). Superoxide dismutase from *Bacillus stearothermophilus*: Crystallization and preliminary X-ray diffraction studies. *J. Mol. Biol. 105*, 333–335.

Brünger, A.T. (1992a). X-PLOR 3.0. Yale University, New Haven, Connecticut.

Brünger, A.T. (1992b). The free R value: A novel statistical quantity for assessing the accuracy of crystal structures. *Nature 355*, 472–474.

Bull, C., Niederhoffer, E.C., Yoshida, T., & Fee, J.A. (1985). Steady-state kinetic studies of superoxide dismutases: Properties of the iron containing protein from *Escherichia coli*. *J. Am. Chem. Soc. 107*, 3295–3304.

Bull, C. & Fee, J.A. (1991). Kinetic studies of superoxide dismutases: Properties of the manganese containing protein from *Thermus thermophilus*. *J. Am. Chem. Soc. 113*, 4069–4076.

Cambillau, C. & Horjales, E. (1987). TOM: A FRODO superpackage for protein–ligand fitting with energy minimization. *J. Mol. Graph. 5*, 174–177.

Carlioz, A., Ludwig, M.L., Stallings, W.C., Fee, J.A., Steinman, H.M., & Touati, D. (1988). Iron superoxide dismutase: Nucleotide sequence of the gene from *Escherichia coli* K12 and correlation with crystal structures. *J. Biol. Chem. 263*, 1555–1562.

Chan, V.W.F., Bjerrum, M.J., & Borders, C.L., Jr. (1990). Evidence that chemical modification of a positively charged residue at position 189 causes the loss of catalytic activity of iron containing and manganese containing superoxide dismutases. *Arch. Biochem. Biophys. 279*, 195–201.

Crowther, R.A. (1972). The fast rotation function. In *The Molecular Replacement Method* (Rossmann, M.G., Ed.), pp. 173–178. Gordon and Breach, New York.

Crowther, R.A. & Blow, D.M. (1967). A method of positioning a known molecule in an unknown crystal structure. *Acta Crystallogr. 23*, 544–548.

Deutsch, H.F., Hoshi, S., Matsuda, Y., Suzuki, K., Kawano, K., Kitagawa, Y., Katsube, Y., & Taniguchi, N. (1991). Preparation of human manganese superoxide dismutase by tri-phase partitioning and preliminary crystallographic data. *J. Mol. Biol. 219*, 103–108.

Finzel, B.C. (1987). Incorporation of fast Fourier transforms to speed restrained least-squares refinement of protein structures. *J. Appl. Crystallogr. 20*, 53–55.

Fitzgerald, P.M.D. (1988). MERLOT, an integrated package of computer programs for the determination of crystal structure by molecular replacement. University of Alberta, Edmonton, Alberta, Canada.

Gorecki, M., Beck, Y., Hartman, J., Fischer, M., Weiss, L., Tachner, Z., Slavin, S., & Nimrod, A. (1991). Recombinant human superoxide dismutases: Production and therapeutical uses. *Free Radicals Res. Commun. 12–13*, 401–410.

Hendrickson, W.A. & Konnert, J.H. (1980). Incorporation of stereochemical information into crystallographic refinement. In *Computing in Crystallography* (Diamond, R., Ramasehan, S., & Venkatesan, K., Eds.), pp. 13.01–13.23. Indian Academy of Sciences, Bangalore, India.

Hope, H. (1988). Cryocrystallography of biological macromolecules: A generally applicable method. *Acta Crystallogr. B 44*, 22–26.

Jones, T.A. (1978). A graphics model building and refinement system for macromolecules. *J. Appl. Crystallogr. 11*, 268–272.

Kabsch, W. & Sander, C. (1983). Dictionary of protein secondary structure: Pattern recognition of hydrogen-bonded and geometrical features. *Biopolymers 22*, 2577–2637.

Klug-Roth, D., Fridovich, I., & Rabani, J. (1973). Pulse radiolytic investigations of superoxide catalyzed disproportionation. Mechanism for bovine superoxide dismutase. *J. Am. Chem. Soc. 95*, 2786–2790.

Lattman, E.E. & Love, W.E. (1972). A rational search procedure for detecting a known molecule in a crystal. *Acta Crystallogr. B 26*, 1854–1857.

Ludwig, M.L., Metzger, A.L., Pattridge, K.A., & Stallings, W.C. (1991). Manganese superoxide dismutase from *Thermus thermophilus*. A structural model refined at 1.8 Å resolution. *J. Mol. Biol. 219*, 335–358.

Matsuda, Y., Higashiyama, S., Kijime, Y., Suzuki, K., Kawano, K., Akiyama, M., Kawata, S., Taruui, S., Deutsch, H.F., & Taniguchi, N.

(1990). Human liver manganese superoxide dismutase. Purification and crystallization, subunit association and sulfhydryl reactivity. *Eur. J. Biochem. 194*, 77–83.

McAdam, M.E., Fox, R.A., Lavelle, F., & Fielden, E.M. (1977). A pulse-radiolysis study of the manganese-containing superoxide dismutase from *Bacillus stearothermophilus*. A kinetic model for the enzyme action. *Biochem. J. 165*, 71–79.

McCord, J.M. (1988). Free radicals and myocardial ischemia: Overview and outlook. *J. Free Radicals Biol. Med. 4*, 9–14.

McCord, J.M., Boyle, J.A., Day, E.D., Rizzolo, L.J., & Salin, M.L. (1977). A manganese-containing superoxide dismutase from human liver. In *Superoxide and Superoxide Dismutases* (Michelson, A.M., McCord, J.M., & Fridovich, I., Eds.), pp. 129–138. Academic Press, New York.

Miller, S. (1989). The structure of interfaces between subunits of dimeric and tetrameric proteins. *Protein Eng. 3*, 77–83.

Parizada, B., Werber, M.M., & Nimrod, A. (1991). Protective effects of human recombinant MnSOD in adjuvant arthritis and bleomycin-induced lung fibrosis. *Free Radicals Res. Commun. 15*, 297–301.

Parker, M.W. & Blake, C.C. (1988). Crystal structure of manganese superoxide dismutase from *Bacillus stearothermophilus* at 2.4 Å resolution. *J. Mol. Biol. 199*, 649–661.

Pflugrath, J.W., Saper, M.A., & Quiocho, F.A. (1984). New generation graphics system for molecular modeling. In *Crystallographic Computing* (Hall, S. & Ashida, T., Eds.), pp. 404–407. Clarendon Press, Oxford, UK.

Priestle, J.P. (1988). RIBBON: A stereo cartoon drawing program for proteins. *J. Appl. Crystallogr. 21*, 572–576.

Read, R.J. (1990). Structure-factor probabilities for related structures. *Acta Crystallogr. A 46*, 900–912.

Ringe, D., Petsko, G.A., Yamakura, F., Suzuki, K., & Ohmori, D. (1983). Structure of iron superoxide dismutase from *Pseudomonas ovalis* at 2.8 Å resolution. *Proc. Natl. Acad. Sci. USA 80*, 3879–3883.

Rossmann, M.G. & Blow, D.M. (1962). The detection of sub-units within the crystallographic asymmetric unit. *Acta Crystallogr. 15*, 24–31.

Sato, S. & Nakazawa, K. (1978). Purification and properties of superoxide dismutase from *Thermus thermophilus* HB8. *J. Biochem. 83*, 1165–1171.

Sheriff, S. (1987). Addition of symmetry-related contact restraints to PROTIN and PROLSQ. *J. Appl. Crystallogr. 20*, 55–57.

Stallings, W.C., Metzger, A.L., Pattridge, K.A., Fee, J.A., & Ludwig, M.L. (1991). Structure-function relationships in Fe and Mn-superoxide dismutases. *Free Radicals Res. Commun. 12–13*, 259–268.

Stallings, W.C., Pattridge, K.A., Strong, R.K., & Ludwig, M.L. (1984). Manganese and iron superoxide dismutases are structural homologs. *J. Biol. Chem. 259*, 10695–10699.

Stallings, W.C., Pattridge, K.A., Strong, R.K., & Ludwig, M.L. (1985). The structure of manganese superoxide dismutases from *Thermus thermophilus* at 2.4 Å resolution. *J. Biol. Chem. 260*, 16424–16432.

Stallings, W.C., Powers, T.B., Pattridge, K.A., Fee, J.A., & Ludwig, M.L. (1983). Iron superoxide dismutase from *Escherichia coli* at 3.1 Å resolution: A structure unlike that of copper/zinc protein at both monomer and dimer levels. *Proc. Natl. Acad. Sci. USA 80*, 3884–3888.

Steigemann, W. (1985). PROTEIN, a program system for the crystal structure analysis of proteins. Max-Planck-Institut, Martinsried, Germany.

Steinman, H. (1982). Superoxide dismutases: Protein chemistry and structure-function relationships. In *Superoxide Dismutase*, Vol. I (Oberley, L.W., Ed.), pp. 11–68. CRC Press, Boca Raton, Florida.

Stoddard, B.L., Howell, P.L., Ringe, D., & Petsko, G.A. (1990). The 2.1 Å structure of iron superoxide dismutase from *Pseudomonas ovalis*. *Biochemistry 29*, 8885–8893.

Sussman, J.L., Holbrook, S.R., Church, G.M., & Kim, S.H. (1977). A structure factor least squares refinement procedure for macromolecular structures using constraints and restrained parameters. *Acta Crystallogr. A 33*, 800–804.

Tainer, J.A., Getzoff, E.D., Beem, K.M., Richardson, J.S., & Richardson, D.C. (1982). Determination of the 2.0 Å structure of copper, zinc superoxide dismutase. *J. Mol. Biol. 160*, 181–217.

Wagner, U.G., Werber, M.M., Beck, Y., Hartman, J.R., Frolow, F., & Sussman, J.L. (1989). Characterization of crystals of genetically engineered human manganese superoxide dismutase. *J. Mol. Biol. 206*, 787–788.

Ward, K.B., Wishner, B.C., Lattman, E.E., & Love, W.E. (1975). Structure of deoxyhemoglobin A. Crystals grown from polyethylene gylcol solutions. *J. Mol. Biol. 98*, 161–177.

Werber, M.M. & Greenstein, L.A. (1991). Biochemical and stability properties of recombinant human MnSOD. *Free Radicals Res. Commun. 12–13*, 335–348.